Endothelial dysfunction and inflammation in diabetic nephropathy

Bus, P.

Chapter 2

Apolipoprotein C-I plays a role in the pathogenesis of glomerulosclerosis

Pascal Bus, Louise Pierneef, Rosalie Bor, Ron Wolterbeek, Leendert A. van Es, Patrick C.N. Rensen, Emile de Heer, Louis M. Havekes, Jan A. Bruijn, Jimmy F. Berbée, and Hans J. Baelde

The Journal of Pathology. Apr 2017; 241(5):589-599

Abstract

Diabetic nephropathy is the leading cause of end-stage renal disease. Diabetic patients have increased plasma concentrations of apolipoprotein C-I (apoCI), and meta-analyses found that a polymorphism in *APOC1* is associated with an increased risk of developing nephropathy. To investigate whether overexpressing apoCI contributes to the development of kidney damage, we studied renal tissue and peritoneal macrophages from *APOC1* transgenic (*APOC1*-tg) mice and wild-type littermates. In addition, we examined renal material from autopsied diabetic patients with and without diabetic nephropathy and from autopsied control subjects. We found that *APOC1*-tg mice, but not wild-type mice, develop albuminuria, renal dysfunction, and glomerulosclerosis with increased numbers of glomerular M1 macrophages. Moreover, compared to wild-type macrophages, stimulated macrophages isolated from *APOC1*-tg mice have increased cytokine expression, including TNF-alpha and TGF-beta, both of which are known to increase the production of extracellular matrix proteins in mesangial cells. These results suggest that *APOC1* expression induces glomerulosclerosis, potentially by increasing the cytokine response in macrophages. Furthermore, we detected apoCI in the kidneys of diabetic patients, but not in control kidneys. Moreover, patients with diabetic nephropathy have significantly more apoCI present in glomeruli compared to diabetic patients without nephropathy, suggesting that apoCI could be involved in the development of diabetic nephropathy. ApoCI co-localized with macrophages. Therefore, apoCI is a promising new therapeutic target for patients at risk of developing nephropathy.

Introduction

Diabetic nephropathy (DN) is the leading cause of end-stage renal disease in the Western world[1]. Several factors contribute to the development of DN, including hyperglycaemia[2], hypertension[3], hyperlipidaemia[4], and genetic background[5]. Meta-analyses revealed that a polymorphism in the *APOC1* gene, which encodes apolipoprotein C-I, is associated with an increased risk of developing DN[6,7]. Moreover, a recent study reported that patients with either type 1 or type 2 diabetes have higher plasma levels of apoCI compared to non-diabetic controls[8].

In the circulation, apolipoproteins are found primarily on the surface of lipid complexes called lipoproteins (e.g., chylomicrons, very-low-density lipoproteins, and high-density lipoproteins). Apolipoproteins regulate the metabolism of lipoproteins, thereby determining the transport and redistribution of lipids among various tissues. Lipoprotein catabolism is dependent on both the apolipoproteins present on their surface and the proteins—including enzymes and receptors—with which they interact. ApoCI slows the catabolism of triglyceride-rich lipoproteins primarily by inhibiting the enzyme lipoprotein lipase (LPL), thereby increasing plasma triglycerides[9]. In addition, apoCI has inflammatory properties, as it can stimulate the production of TNF-alpha by macrophages following an inflammatory stimulus[10].

Studies performed in both human subjects and animal models revealed that macrophages play an important role in the pathogenesis of DN[11-17], and macrophage-derived TNF-alpha is believed to be a key mediator of this process[17]. Several studies regarding the role of macrophages in DN found increased number of macrophages both in glomeruli and in the interstitium. This influx of macrophages is correlated with glomerular and tubulointerstitial damage and with a decline in renal function[11-16,18,19]. Reciprocally, suppressing macrophage influx markedly reduces urinary albumin secretion, glomerular hypertrophy, and mesangial matrix expansion[14,20,21].

We hypothesise that increased expression of apoCI plays an important role in the development of kidney damage, based on three key findings: *i)* the results of the meta-analysis, which showed an association between an *APOC1* polymorphism and the development

of DN; *ii*) the finding that apoCI stimulates the inflammatory response in macrophages; and *iii*) that macrophages are involved in the development of DN. To test this hypothesis, we examined whether human *APOC1* transgenic mice develop kidney damage. Next, we investigated the role of macrophages in this process. Finally, to test whether apoCI is clinically relevant in the development of DN, we investigated the expression of apoCI in the kidneys of patients with and without DN as well as in kidneys from non-diabetic controls.

Materials and methods

Animals

In this study, we used both male and female heterozygous transgenic mice expressing human apolipoprotein C-I (*APOC1*-tg) on a C57Bl/6J background. The construct was generated by the excision of an 18-kb EcoRI fragment from a cosmid carrying the *APOE/APOC1/APOC1P1* gene region. The fragment contained a 5-kb region upstream from *APOC1* and an 8-kb region downstream from *APOC1*, including the hepatic control region element and part of *APOC1P1* pseudogene[22]. Transgenic offspring were identified by polymerase chain reaction (PCR) analysis on genomic tail-derived DNA. Male and female wild-type (WT) littermates were used as controls. Equal numbers of male and female mice were used. All mice used in this study were housed under standard laboratory conditions with free access to water and standard rodent chow (Hope Farms, Woerden, the Netherlands).

Experimental design

All animal experiments were approved by the Institutional Ethics Committee for Animal Care and Experimentation. To measure the animals' characteristics, WT and *APOC1*-tg mice (10 mice per group) were sacrificed at six months of age. The kidneys, heart, liver, brain, lungs, spleen, and pancreas were collected, and both absolute and relative weights were measured. From each organ, one piece was fixed in 4% buffered formalin and embedded in paraffin, and one piece was snap-frozen for mRNA isolation. Blood was collected in heparin tubes and used to measure white blood cells (WBCs) and haemoglobin

concentration. Blood plasma was used to measure triglycerides (TGs), total cholesterol (TC), high-density lipoprotein cholesterol (HDL-C), non-HDL-C, glutamate oxaloacetate transaminase (GOT), creatinine kinase (CK), and glucose levels. Serum was used to measure blood urea nitrogen (BUN) and serum creatinine. WBCs were counted using a Muse Cell Counter (Merck, Darmstadt, Germany). A BUN colorimetric detection kit (Arbor Assays, Ann Arbor, MI, USA) was used in accordance with the manufacturer's instructions. Serum creatinine was measured using an enzymatic method on a Roche Modular P800 device (Roche, Woerden, the Netherlands) in accordance with the manufacturer's instructions. Haemoglobin, GOT, and CK were measured using Reflotron Sprint (Roche) test strips in accordance with the manufacturer's instructions. Serum creatinine was measured using an enzymatic/fluorometric creatinine assay kit (Abcam, Cambridge, UK). Plasma TGs and TC were assayed using commercially available enzymatic kits (Roche Diagnostics, Germany), and plasma glucose was measured using the glucose start reagent method (Instruchemie, Delfzijl, the Netherlands) in accordance with the manufacturer's instructions. HDL-C was measured by precipitating apoB-containing particles with 20% polyethylene glycol in 200 mM glycine buffer (pH 10), and TC was measured in the supernatant. Non-HDL-C was calculated by subtracting HDL-C from TC.

APOC1-tg mice (n=59) and age-matched WT littermates (n=19) were sacrificed at various ages ranging from 2 to 23 months. Subsequently, the kidneys were removed and subjected to histological, immunohistochemical, and mRNA analyses. From each kidney, one piece of cortical tissue was snap-frozen in pre-cooled methylbutane; a second piece was fixed in 4% buffered formalin and embedded in paraffin for histological analysis and immunohistochemistry. Frozen renal cortex samples (30 mg) from three WT and three *APOC1*-tg mice at 16 months of age were used to measure cholesterol, triglyceride, and phospholipid content as described previously for liver tissue[23].

Albuminuria

Urine albumin levels were measured using rocket immunoelectrophoresis against rabbit anti-mouse albumin, with purified mouse serum albumin (Sigma-Aldrich, Saint Louis, MO) as a standard. Urine

creatinine was measured using a creatinine assay, with picric acid, sodium hydroxide, and creatinine standards (Sigma-Aldrich). The rabbit anti-mouse albumin antibody was produced in our laboratory by immunising rabbits with an emulsion of mouse albumin and Freund's adjuvant; specificity was confirmed using western blot analysis. Serum creatinine and BUN were measured in accordance with the manufacturers' instructions (Roche and Arbor Assays, respectively) in 16-month-old mice as a measure of renal function.

Immunohistochemistry

Frozen kidney sections (3-µm thickness) were cut on a Reichert cryostat microtome. Goat anti-human apoCI (Academy Biomedical Company, Houston, TX, USA), rabbit anti-human fibronectin (Sigma-Aldrich), rabbit anti-human collagen VI (Telios Pharmaceuticals, San Diego, CA, USA), goat anti-human collagen types I, III, and IV (all from Sera Laboratories, West Sussex, UK), rat anti-VCAM-1 (Abcam), rat anti-MCP1 (Abcam), rat anti-ICAM (Abcam), rat anti-FA-11 (Abcam), rabbit anti-TNF-alpha (Abcam), rabbit anti-CD11b (Abcam), or rabbit anti-CD163 (Santa Cruz Biotechnology, Dallas, TX, USA) primary antibodies were used for immunostaining, followed by the appropriate HRP-labelled secondary antibody with diaminobenzidine as the chromogen. Double-label immunofluorescence was performed with rat anti-VCAM-1 and goat anti-von Willebrand factor (Affinity Biologicals Inc., Ancaster, Canada), followed by the appropriate fluorescent secondary antibodies, after which the slides were mounted using Vectashield plus DAPI (Vector Laboratories, Burlingame, CA, USA). Double-label immunostaining was performed with goat anti-human apoCI and mouse anti-CD68 (Dako, Glostrup, Denmark), followed by the appropriate secondary antibodies with diaminobenzidine and Vector Blue (Vector Laboratories) as the chromogens for detecting apoCI and CD68, respectively. Frozen kidney sections (10 µm thickness) of 16-month-old WT and *APOC1*-tg mice were stained with oil red O. Paraffin-embedded kidney sections (4 µm thickness) were stained with methenamine silver, periodic acid-Schiff (PAS), or Sirius red (supplementary material, Supplementary material and methods). Sections were immunostained with rabbit anti-WT1 (Abcam) or rat anti-F4/80 (Abcam) primary antibodies, followed by the appropriate HRP-labelled secondary antibody

with diaminobenzidine as the chromogen. The anti-human antibodies used for staining mouse tissue are cross-reactive with mouse tissue (data not shown).

Staining quantification

The number of podocytes in each sample was determined by counting the number of WT1-positive nuclei in 25 glomeruli. Glomerular damage was scored morphologically on PAS-stained tissues in 25 glomeruli, using a scale of 0–4 as follows: 0, normal glomeruli; 1, <10% mesangial expansion; 2, 10-25% glomerulosclerosis; 3, 25-50% glomerulosclerosis; 4, >50% glomerulosclerosis[24]. Sections were scanned, and the images were digitised using a Philips Ultra-Fast Scanner 1.6 RA (Philips Digital Pathology, Best, The Netherlands). The levels of VCAM-1, ICAM-1, and TNF-alpha expression per glomerulus were determined by measuring the surface stained by the respective antibody, relative to the total surface area of the glomerulus (ten glomeruli per section were measured) at 40X magnification (ImageJ). FA-11–positive cells were counted in 10 glomeruli per sample. PAS-stained slides were used to measure the surface area of the glomerular tuft (i.e. glomerular surface area, in μm^2) in 25 glomeruli per sample using Philips Ultra-Fast Scanner 1.6 RA software. Interstitial fibrosis was determined by measuring the surface area stained by Sirius red in five cortical fields (using a 40X objective with a fluorescence microscope) relative to the total surface area of the cortical fields (ImageJ software). Glomeruli and vessels were excluded from the analysis.

Human APOC1 and mouse apoCI expression in *APOC1*-tg mice

RNA was extracted using RNA extraction buffer (TRIzol, Ambion) from kidney, liver, brain, heart, lung, spleen, and pancreas tissues of *APOC1*-tg and WT mice, and from the liver tissue of streptozotocin (STZ)-induced diabetic WT mice 4 months after STZ injection. *APOC1* and *ApoC1* mRNA levels were measured using quantitative real-time PCR.

Macrophage isolation

WT and *APOC1*-tg mice (n=3 each) were given an intraperitoneal injec-

tion of 1 ml thioglycolate (30 g/l) on day 1 in order to increase the macrophage yield. On day 5, after the mice were sacrificed, 6 ml of sterile PBS was used for vigorous peritoneal lavage. The resulting cell suspension was centrifuged at 500 rpm for 10 min and then washed twice with PBS. The cell pellets were resuspended in 2 ml RPMI 1640 medium containing 10% FCS and 1% penicillin/streptomycin (referred to hereafter as 'medium'). The macrophages were counted in a counting chamber, and the cells were then incubated overnight in a six-well plate (with 500.000 macrophages per well in 1.2 ml of medium). After the cells were washed with medium, they were incubated for 6 h at 37˚C in the following conditions: no stimulation; 10 ng/ml LPS[25]; or 10 ng/ml LPS and 10 ng/ml anti-CD14 antibody (Zimmer Biomet, Warsaw, IN, USA). After 6 h, the medium was collected and the cells were washed three times with PBS and then dissolved in 1 ml TRIzol.

Reverse transcription and CDNA amplification

Quantitative real-time PCR (qRT-PCR) reactions were prepared using SYBR Green I master mix (Bio-Rad, Hercules, CA, USA) as recommended by the manufacturer and run on a Bio-Rad CFX real-time system. Ct (cycle threshold) values were normalised to the housekeeping gene *Hprt1*. The primer sequences used in this study are provided in the supplementary material, Supplementary materials and methods.

Human kidney samples

Renal tissue specimens were obtained from autopsy samples collected from 17 control subjects without diabetes or renal disease, from 8 patients with diabetes without nephropathy, and from 12 patients with nodular glomerulosclerosis (class III DN, based on the established histopathological classification for DN)[26]. Autopsy samples were retrieved from the pathology archives at Leiden University Medical Center. The non-diabetic control subjects, diabetic patients without nephropathy, and diabetic patients with nephropathy were 65±12, 76±12, and 72±9 years of age, respectively (p=0.086). The duration of diabetes did not differ significantly between the two diabetic groups (p=0.13).

Statistics

Because animals were randomly sacrificed between 2 and 23 months

of age, and because the relationship between glomerular damage and age produced a sigmoid-like curve for the *APOC1*-tg mice (compared to a linear relationship for the WT mice), we analysed our data by dividing mice into three age categories: ≤8 months, 8–16 months, and >16 months. We studied the various outcomes using two-way ANOVAs with an interaction term between age and genotype in the model. Model fit was assessed by visual inspection of residuals of the ANOVA models. Patient data and *in vitro* experiments were analysed using the two-tailed Student's *t* test. Differences were considered significant at $p<0.05$.

Results

Human *APOC1* transgenic mice develop glomerulosclerosis

The animals' baseline characteristics were measured at 6 months of age and are summarised in the supplementary material, Tables S1 and S2. The absolute organ weights did not differ significantly between WT and *APOC1*-tg mice; however, the relative organ weights of the kidneys and heart were significantly higher in the *APOC1*-tg mice. The *APOC1*-tg mice had hyperlipidaemia, with increased serum levels of triglycerides, total cholesterol, and non-HDL-C ($p<0.001$). In the *APOC1*-tg mice, the human *APOC1* transgene is primarily expressed in the liver and, to a lesser extent, peritoneal macrophages (Figure 1A). Accordingly, human apoCI protein was present primarily in the liver; in other organs, human apoCI protein was restricted to the blood vessels (Figure 1B-H). The liver mRNA levels of mouse *ApoC1* were 2.8-fold higher in STZ-induced diabetic mice than in WT mice ($p<0.05$; Figure 1I).

To examine whether *APOC1*-tg mice develop albuminuria, we next measured the urinary albumin:creatinine ratio at various ages (Figure 2). Compared with WT mice, the albumin:creatinine ratio was significantly higher in *APOC1*-tg mice from 14 months of age ($p<0.05$). In addition, at 16 months of age serum creatinine levels were 2.7-fold-higher in the *APOC1*-tg mice than in WT mice ($p<0.05$; data not shown). Blood urea nitrogen (BUN) levels did not differ significantly between *APOC1*-tg mice and WT mice at 16 months of age (data not shown).

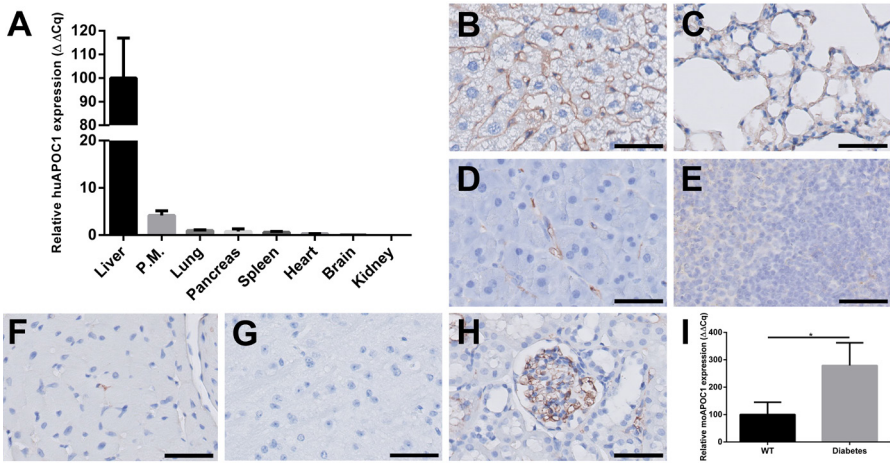

Figure 1: Transgenic mRNA and protein levels in *APOC1*-tg mice. A. Relative mRNA levels (ΔΔCq) of human *APOC1* in the organs and peritoneal macrophages (P.M.) of 6-month-old *APOC1*-tg mice. Human *APOC1* mRNA level in the liver was set to 100%. B-H. Representative images of human apoCI-immunostained liver (B), lung (C), pancreas (D), spleen (E), heart (F), brain (G), and kidney (H) samples from a 6-month-old *APOC1*-tg mouse. I. Relative mRNA levels (ΔΔCq) of mouse *ApoC1* in the liver of 6-month-old WT and STZ-induced diabetic mice. WT liver mouse *ApoC1* mRNA level was set to 100%. Scale bars indicate 50 μm.

Next, we examined the morphology of the glomeruli in *APOC1*-tg and WT mice in three age categories. Interaction effects for age and genotype were found for the glomerular damage score, glomerular hypertrophy, and the number of podocytes ($p<0.001$). At 9 months of age, the *APOC1*-tg mice began to develop mesangial matrix expansion (Figure 3B); by 15 months, this had progressed to glomerulosclerosis and was accompanied by glomerular hypertrophy (Figure 3I, J). These glomerulosclerotic lesions have a nodular-like pattern (Figure 3D) and were positive for several extracellular matrix (ECM) proteins, including collagen type I, collagen type IV, and fibronectin (supplementary material, Figure S1A-C). Lesions were also positive for collagen type VI; however, this protein was observed primarily at the periphery of the sclerotic lesions (supplementary material, Figure S1D). Decreased number of podocytes is a common feature in several kidney diseases, including DN[27]. Consistent with this finding, the number of podocytes

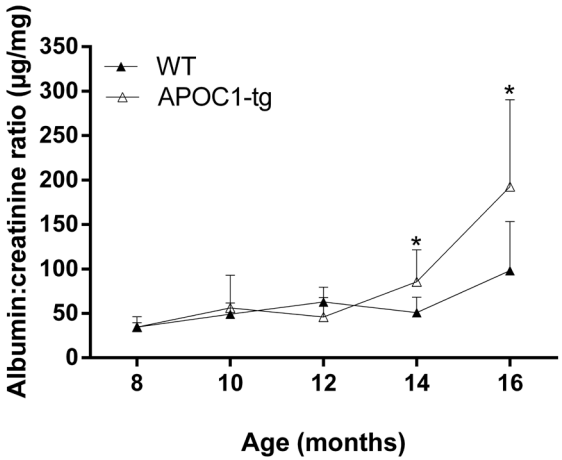

Figure 2: Time course of urinary albumin:creatinine ratio in WT and *APOC1*-tg mice. **p*<0.05, Student's *t* test.

generally decreased with age in *APOC1*-tg mice (Figure 3E, F, K). WT mice displayed no sign of either mesangial matrix expansion (Figure 3A, C, I) or podocyte loss at any time point studied (Figure 3K). Sirius red staining combined with fluorescence microscopy revealed that interstitial fibrosis increased significantly during ageing in both WT and *APOC1*-tg mice ($p<0.01$). Compared to WT mice, *APOC1*-tg mice developed significantly more interstitial fibrosis ($p<0.05$; Figure 3G, H, L). In the *APOC1*-tg mice, interstitial fibrosis was correlated with the number of podocytes ($r=-0.630$; $p<0.001$), glomerular damage ($r=0.485$; $p<0.001$), glomerular hypertrophy ($r=0.358$; $p<0.001$), and the number of glomerular macrophages ($r=0.492$; $p<0.001$). In contrast, the animals' sex was not correlated with glomerular damage ($p=0.939$), the number of podocytes ($p=0.486$), glomerular hypertrophy ($p=0.973$), or interstitial fibrosis ($p=0.542$). We also found no significant difference between *APOC1*-tg and WT mice at 16 months of age with respect to renal cortex triglyceride (3.9±0.4 and 4.6±1.7 nmol/mg tissue, respectively), total cholesterol (10.7±3.1 and 9.8±0.3 nmol/mg tissue, respectively), or phospholipid (24.3±7.4 and 22.9±0.7 nmol/mg tissue, respectively) levels. In addition, oil red O staining revealed no significant difference in renal lipid deposition between *APOC1*-tg and WT mice at 16 months of age (data not shown).

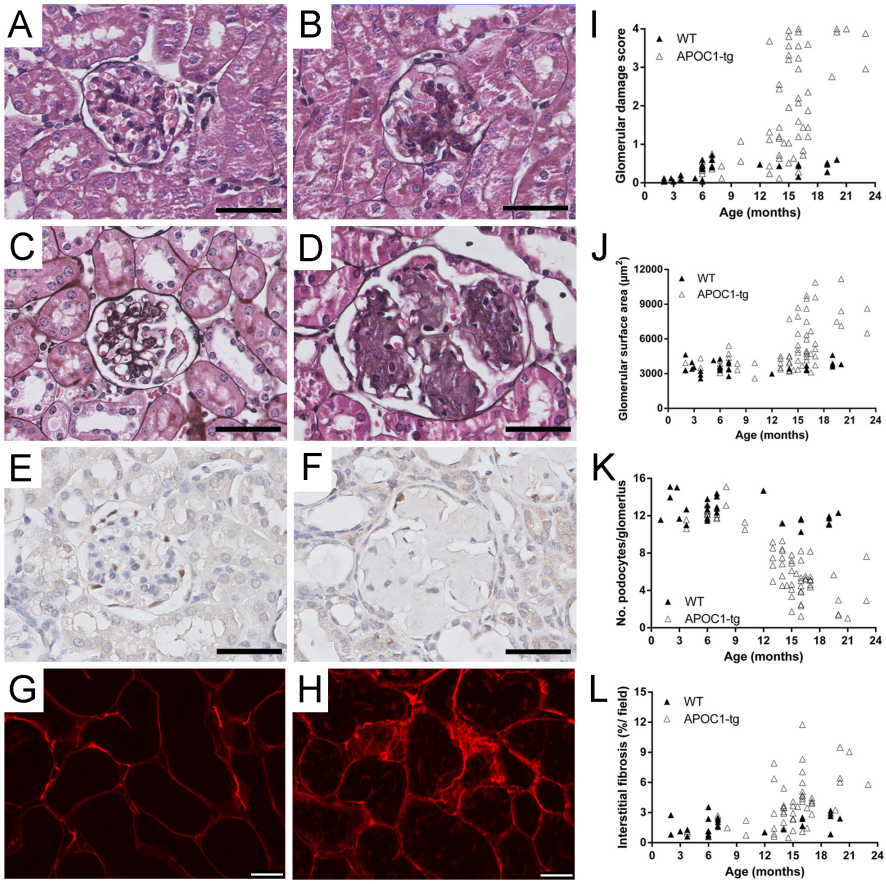

Figure 3: ***APOC1*-tg mice develop glomerulosclerosis and interstitial fibrosis.** A and C. WT mice have normal glomerular morphology at 4 months (A) and 16 months (C) of age. B and D. *APOC1*-tg mice develop kidney damage with ageing, evident as mesangial matrix expansion beginning at 9 months of age (B); this expansion progressed to severe glomerulosclerosis by 15 months of age (D). E-F. The number of podocytes decreases with age in *APOC1*-tg mice, beginning at 13 months of age (E); by 20 months, extremely few podocytes remain (F). G-H. At 20 months of age, *APOC1*-tg mice (H) develop significantly more interstitial fibrosis than age-matched WT mice (G). I. Glomerular damage score plotted against age. J. Glomerular surface area plotted against age. K. The number of podocytes per glomerulus plotted against age. L. Interstitial fibrosis per field plotted against age. The sections shown in A-D were stained with methenamine silver. The sections shown in E-F were immunostained for WT1, a marker for podocytes, and the sections shown in G-H were stained with Sirius red. Scale bars indicate 50 µm (A-F) and 25 µm (G-H).

Influx of inflammatory M1 macrophages in *APOC1*-tg mice

Next we examined whether macrophages might be responsible for the development of glomerulosclerosis in *APOC1*-tg mice. Again, we separated mice into three age categories for analysis. Even in the youngest (≤8 months) *APOC1*-tg mice had more glomerular macrophages than their WT littermates (Figure 4A, B) ($p<0.01$). This difference in glomerular macrophages in favour of *APOC1*-tg mice over WT mice remained significant across the age categories ($p<0.01$) (Figure 4C, D, K). Male and female mice did not differ with respect to the number of glomerular macrophages ($p=0.651$). Positive staining for CD11b and FA-11 on adjacent slides[28], combined with negative staining for CD163, indicates that the glomerular macrophages in *APOC1*-tg mice are M1 inflammatory macrophages. In addition, the glomeruli in *APOC1*-tg mice had greater levels of TNF-alpha than WT glomeruli ($p<0.001$) (Figure 4E, F, L), supporting the presence of M1 macrophages. Both VCAM-1 (Figure 4G, H, M) and ICAM-1 (Figure 4I, J, N) were up-regulated in *APOC1*-tg mice as early as 4 months of age, suggesting that both adhesion molecules play a role in the influx of glomerular macrophages. Double-staining for VCAM-1 and von Willebrand factor (vWF) revealed that VCAM-1 expression increased exclusively in endothelial cells (supplementary material, Figure S2). A histological examination of ICAM-1 revealed that its expression was also increased in endothelial cells.

ApoCI enhances the inflammatory response

We previously reported that apoCI increases the production of TNF-alpha in LPS-stimulated macrophages[10] by enhancing the binding of LPS to Toll-like receptor 4 (TLR4) via CD14[29]. Based on these results and findings from the present study, we hypothesised that the glomerulosclerosis seen in *APOC1*-tg mice is caused by macrophages expressing human *APOC1*, which leads to an increased cytokine response in these macrophages upon activation, ultimately stimulating mesangial cells to up-regulate production of the ECM. To test this hypothesis, we isolated peritoneal macrophages from both WT and *APOC1*-tg mice, stimulated these cells with LPS, and measured the mRNA expression levels of inflammatory and fibrogenic cytokines. Compared with WT cells, the expression levels of *Tnfa* and *Il1b* (pro-inflammatory

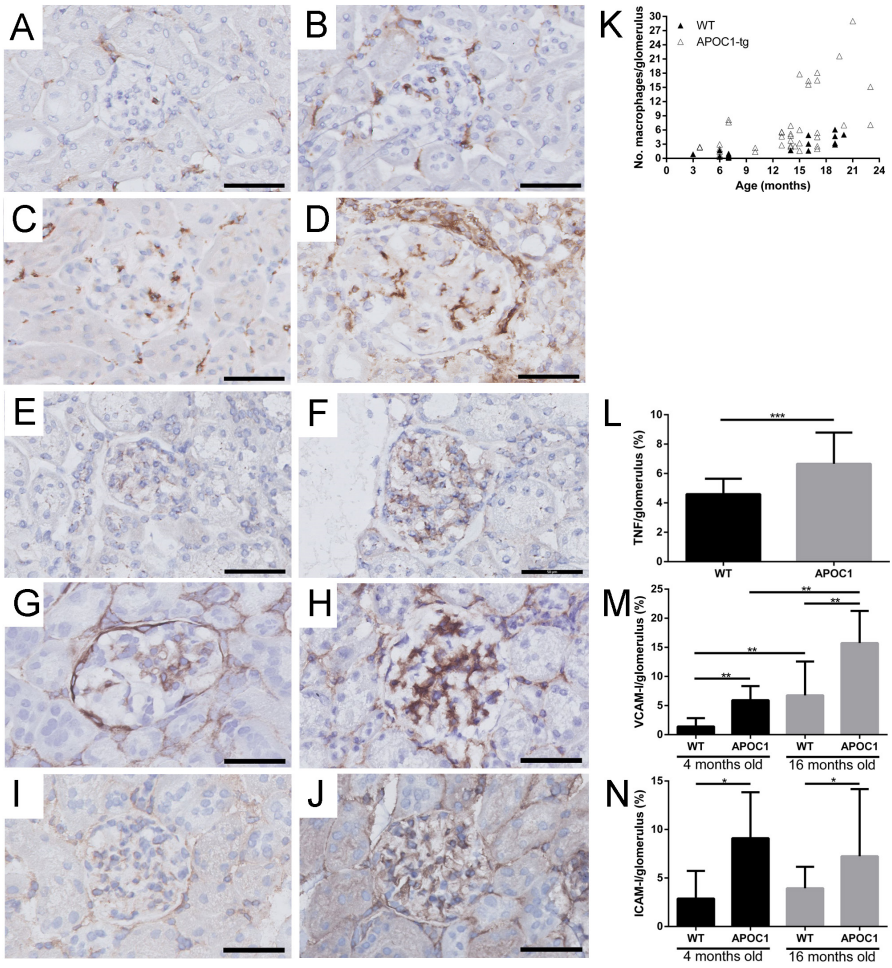

Figure 4: ***APOC1*-tg mice have increased numbers of glomerular macrophages and increased endothelial activation**. A-D. At 4 months (A, B) and 16 months (C, D) of age, *APOC1*-tg mice (B, D) have more glomerular macrophages than WT mice (A, C). E-F. At 16 months of age, TNF-alpha protein levels are higher in *APOC1*-tg mice (F) than in WT mice (E). G-J. At 16 months of age, *APOC1*-tg mice have increased expression of VCAM-1 (H) and ICAM-1 (J) compared with WT mice (G and I, respectively). K. The number of macrophages per glomerulus plotted against age. L. TNF-alpha expression per glomerulus. M. VCAM-1 expression per glomerulus. N. ICAM-1 expression per glomerulus. *p<0.05, **p<0.001, and ***p<0.001, one-way ANOVA. Scale bars indicate 50 µm.

cytokines), and the expression levels of *Tgfb1* and *Pdgfb* (both pro-fibrotic cytokines) were significantly increased in LPS-stimulated *APOC1*-tg macrophages, as well as the expression level of *Tlr4* (Figure 5). Incubating macrophages with LPS and anti-CD14 antibodies prevented the increased expression of cytokines in *APOC1*-tg macrophages (Figure 5), consistent with previous data that apoCI enhances the biological response to LPS via the CD14/TLR4 pathway[29].

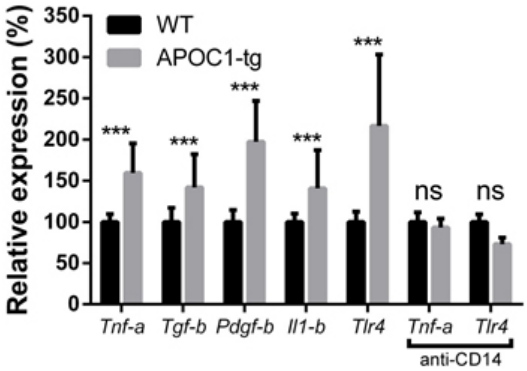

Figure 5: ***APOC1*-tg macrophages have an increased cytokine response**. Macrophages were isolated from wild-type (WT) or *APOC1*-tg mice and stimulated with LPS (10 ng/ml) or LPS and anti-CD14 (10 ng/ml) for 6 h at 37°C. The mRNA levels of *Tnf-alpha*, *Tgf-beta*, *Pdgf-beta*, *Il1-beta*, and *Tlr4* were measured. The expression levels were normalised to the respective LPS-stimulated WT control and are expressed as the mean ± sd. ***p<0.001, Student's t test.

Patients with DN have increased expression of glomerular apoCI

As a first step towards testing the hypothesis that apoCI plays a role in human DN, we studied the presence of apoCI in glomeruli of non-diabetic subjects and diabetic patients with and without DN. The patient characteristics are summarised in the supplementary material, Table S3. The glomeruli in non-diabetic controls were generally negative for apoCI (Figure 6A). In contrast, the glomeruli of kidneys obtained from diabetic patients were positive for apoCI (Figure 6B, C). The percentage of apoCI-positive glomeruli was greater in diabetic patients with nephropathy than in those without nephropathy (Figure 6D). Double-label immunostaining revealed that apoCI co-localizes with macrophages. In addition, apoCI was present in resident renal cells (Figure 6E-G).

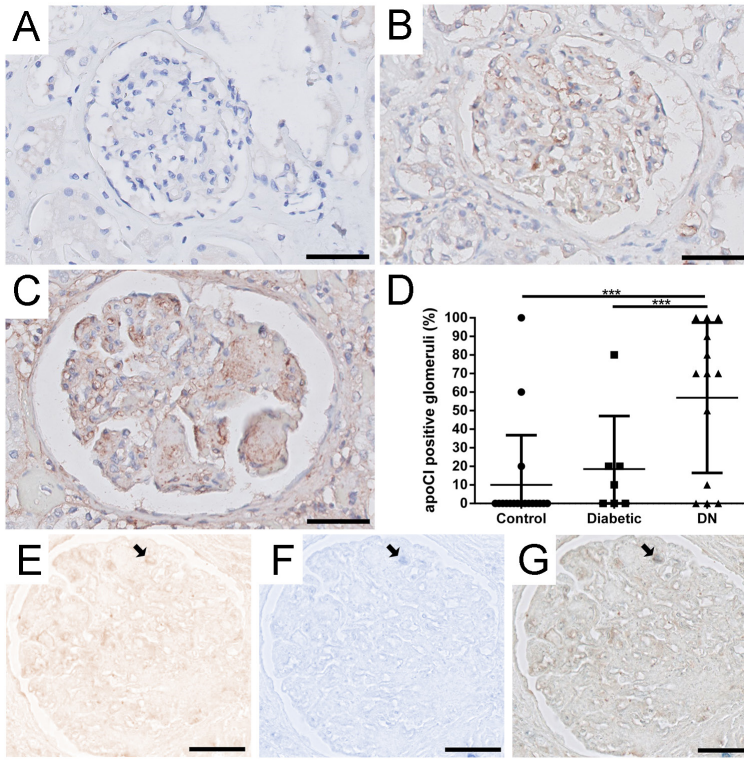

Figure 6: **Patients with DN have increased expression of glomerular apoCI**. A. Representative kidney section from a control subject showing no glomerular apoCI staining. B. Representative kidney section from a patient with diabetes without nephropathy, positive for apoCI. C. Representative kidney section from a patient with diabetes and nephropathy. D. The percentage of apoCI-positive glomeruli in control subjects and diabetic patients with and without DN. E-G. Double-label immunostaining for apoCI (E) and CD68 (F) shows co-localization of apoCI with CD68-positive macrophages (arrows); Panel G shows a merged image. ApoCI is also present in resident renal cells. ***p<0.001, one-way ANOVA. Scale bars indicate 50 µm.

Discussion

Here, we report that transgenic mice expressing the human *APOC1* gene develop glomerulosclerosis and renal dysfunction with increased albuminuria beginning at 14 months of age. The degree of kidney damage was correlated strongly with age, glomerular hypertrophy,

reduced podocyte numbers, and the number of glomerular macrophages. Moreover, apoCI increased the expression of inflammatory and fibrogenic cytokines in macrophages upon stimulation *in vitro*. Our finding that renal cortex lipid content – specifically, triglycerides, total cholesterol, and phospholipids – does not differ between *APOC1*-tg mice and WT mice suggests that the development of renal damage in *APOC1*-tg mice is not due to changes in lipid metabolism, but is likely to be due to a different function of apoCI, possibly through the activation of macrophages. This notion is supported by the finding that the increased apoCI concentration in patients with type 2 diabetes (T2D) is only partially explained by increased TG levels in these patients[30]. To further investigate the involvement of *APOC1* in the development of renal damage, we examined whether *APOC1* expression was increased in STZ-induced diabetic WT mice, an animal model for diabetic nephropathy. The mRNA levels of mouse *ApoC1* in the livers of STZ-induced diabetic WT mice were 2.8-fold higher than those in control WT mice, supporting the role of apoCI in DN. These findings are clinically relevant, as they show that apoCI plays a role in the pathogenesis of glomerulosclerosis. Interestingly, we found that, compared with controls, patients with diabetes and DN showed a significant increase in glomerular apoCI expression, supporting our hypothesis that apoCI plays a role in the pathogenesis of glomerulosclerosis in DN. Our double-label immunostaining experiments revealed that apoCI co-localized with macrophages, and apoCI was also present in resident renal cells. Given that the renal cells do not express human *APOC1* mRNA, this indicates that the apoCI present in resident renal cells was taken up either from macrophages or from the circulation.

Bouillet *et al.* recently reported that patients with type 1 diabetes (T1D) develop less nephropathy compared with T2D patients, even though T1D and T2D patients have similar increases in plasma apoCI levels compared with control subjects[8]. It is important to note that Bouillet *et al.* used proteinuria levels as a measure of nephropathy; therefore, it is possible that nephropathy was underdiagnosed. This notion is supported by our recent finding that DN lesions can develop before the onset of clinical findings; specifically, 20 out of 106 patients with histologically confirmed DN did not present with DN-associated clinical manifestations[31].

We propose that apoCI mediates the development of glomerulosclerosis in *APOC1*-tg mice via at least two distinct mechanisms. First, *APOC1* expression results in dyslipidaemia[22,32], which is reported to increase the expression of VCAM-1 and ICAM-1 in glomeruli[33,34]. These proteins mediate monocyte/macrophage infiltration and thereby contribute to the severity of DN. This is supported by the finding that diabetic ICAM-1-deficient mice have reduced glomerular infiltration of macrophages and are protected from developing renal injury[20]. Second, apoCI – either derived from the circulation[10] or expressed by macrophages – increases the inflammatory and fibrogenic response of stimulated macrophages, including increased expression of TNF-alpha and TGF-beta. These cytokines have been reported to increase the expression of ECM proteins in mesangial cells[17,35-38]. In addition to increasing matrix production, both TNF-alpha and TGF-beta downregulate expression of the protein nephrin in podocytes, thereby altering glomerular permeability and leading to albuminuria[39]. TGF-beta also induces apoptosis in podocytes[40].

Glomerular nodules, also known as Kimmelstiel-Wilson nodules, are characteristic of class III DN[26] and may be a form of microangiopathy[41]. *APOC1*-tg mice develop a renal phenotype with nodular glomerulosclerosis, with increased collagen types I, IV, and VI, increased renal dysfunction, increased glomerular hypertrophy, reduced podocyte numbers, and interstitial fibrosis – all of which are reminiscent of DN, even though these mice are not diabetic. These results support our previous finding that DN can develop without clinical manifestations[31]. With the exception of BTBR Ob/Ob mutant mice[16], nodular glomerulosclerosis is generally not observed in mice. In addition to its role in the development of glomerulosclerosis, apoCI also plays a role in the development of atherosclerosis. The apoCI content of triglyceride-rich lipoproteins (TRLs) is an independent predictor of early atherosclerosis[42] and is correlated with plaque size in carotid atherosclerosis[43]. Likewise, we previously reported that endogenous apoCI expression in hyperlipidaemia mice increased the size of atherosclerotic lesions by 60%, and this was related to an increased inflammatory response in macrophages[44]. Moreover, increased apoCI levels in TRL particles are also present in patients with DN[45], and diabetes is known to increase the risk of cardiovascular disease, including atherosclerotic disease

and congestive heart failure[46]. The finding that apoCI is involved in both nodular glomerulosclerosis and atherosclerosis supports the notion that glomerular nodules may be the result of vascular damage.

Taken together, our results obtained from *APOC1*-tg mice and patients with DN provide new insights into the role that apoCI plays in the development of glomerulosclerosis and suggest apoCI as a therapeutic target for slowing the progression of DN in high-risk patients. These data also shed new light on the mechanism by which the inflammatory and fibrogenic response is increased in macrophages, potentially leading to the development of nodular glomerulosclerosis present in *APOC1*-tg mice. Future studies should help determine whether macrophages are indeed the key contributor to the observed renal phenotype and whether *APOC1* affects the development of DN.

Acknowledgements

This study was supported by the Netherlands CardioVascular Research Initiative – the Dutch Heart Foundation, the Dutch Federation of University Medical Centers, the Netherlands Organisation for Health Research and Development, the Royal Netherlands Academy of Sciences – for the GENIUS project 'Generating the best evidence-based pharmaceutical targets for atherosclerosis' (CVON 2011) and the Preventing Diabetes foundation. PCNR is an Established Investigator of the Netherlands Heart Foundation (grant 2009T038). We would like to thank Gabrielle Pinkse, Malu Zandbergen, Kimberley Veraar, and Trea Streefland for technical support.

References

1. Ahmad J. Management of diabetic nephropathy: Recent progress and future perspective. Diabetes Metab Syndr. Mar 6 2015.
2. Stratton IM, Adler AI, Neil HA, et al. Association of glycaemia with macrovascular and microvascular complications of type 2 diabetes (UKPDS 35): prospective observational study. BMJ. Aug 12 2000;321(7258):405-412.
3. Tight blood pressure control and risk of macrovascular and microvascular complications in type 2 diabetes: UKPDS 38. UK Prospective Diabetes Study Group. BMJ. Sep 12 1998;317(7160):703-713.
4. Jaiswal M, Schinske A, Pop-Busui R. Lipids and lipid management in diabetes. Best Pract Res Clin Endocrinol Metab. Jun 2014;28(3):325-338.
5. Borch-Johnsen K, Norgaard K, Hommel E, et al. Is diabetic nephropathy an inherited complication? Kidney Int. Apr 1992;41(4):719-722.
6. Mooyaart AL, Valk EJ, van Es LA, et al. Genetic associations in diabetic nephropathy: a meta-analysis. Diabetologia. Mar 2011;54(3):544-553.
7. McKay GJ, Savage DA, Patterson CC, et al. Association analysis of dyslipidemia-related genes in diabetic nephropathy. PLoS One. 2013;8(3):e58472.
8. Bouillet B, Gautier T, Blache D, et al. Glycation of apolipoprotein C1 impairs its CETP inhibitory property: pathophysiological relevance in patients with type 1 and type 2 diabetes. Diabetes Care. Apr 2014;37(4):1148-1156.
9. Berbee JF, van der Hoogt CC, Sundararaman D, et al. Severe hypertriglyceridemia in human APOC1 transgenic mice is caused by apoC-I-induced inhibition of LPL. J Lipid Res. Feb 2005;46(2):297-306.
10. Berbee JF, van der Hoogt CC, Kleemann R, et al. Apolipoprotein CI stimulates the response to lipopolysaccharide and reduces mortality in gram-negative sepsis. FASEB J. Oct 2006;20(12):2162-2164.
11. Ninichuk V, Khandoga AG, Segerer S, et al. The role of interstitial macrophages in nephropathy of type 2 diabetic db/db mice. Am J Pathol. Apr 2007;170(4):1267-1276.
12. Chow FY, Nikolic-Paterson DJ, Ma FY, et al. Monocyte chemoattractant protein-1-induced tissue inflammation is critical for the development of renal injury but not type 2 diabetes in obese db/db mice. Diabetologia. Feb 2007;50(2):471-480.
13. Chow F, Ozols E, Nikolic-Paterson DJ, et al. Macrophages in mouse type 2 diabetic nephropathy: correlation with diabetic state and progressive renal injury. Kidney Int. Jan 2004;65(1):116-128.
14. Chow FY, Nikolic-Paterson DJ, Ozols E, et al. Intercellular adhesion molecule-1 deficiency is protective against nephropathy in type 2 diabetic db/db mice. J Am Soc Nephrol. Jun 2005;16(6):1711-1722.
15. Sassy-Prigent C, Heudes D, Mandet C, et al. Early glomerular macrophage recruitment in streptozotocin-induced diabetic rats. Diabetes. Mar 2000;49(3):466-475.
16. Hudkins KL, Pichaiwong W, Wietecha T, et al. BTBR Ob/Ob mutant mice model progressive diabetic nephropathy. J Am Soc Nephrol. Sep 2010;21(9):1533-1542.
17. Awad AS, You H, Gao T, et al. Macrophage-derived tumor necrosis factor-alpha mediates diabetic renal injury. Kidney Int. Jun 10 2015.
18. Coimbra TM, Janssen U, Grone HJ, et al. Early events leading to renal injury in obese Zucker (fatty) rats with type II diabetes. Kidney Int. Jan 2000;57(1):167-182.
19. Nguyen D, Ping F, Mu W, et al. Macrophage accumulation in human progressive diabetic nephropathy. Nephrology (Carlton). Jun 2006;11(3):226-231.
20. Okada S, Shikata K, Matsuda M, et al. Intercellular adhesion molecule-1-deficient mice are resistant against renal injury after induction of diabetes. Diabetes. Oct 2003;52(10):2586-2593.
21. Usui HK, Shikata K, Sasaki M, et al. Macrophage scavenger receptor-a-deficient mice are resistant against diabetic nephropathy through amelioration of microinflammation. Diabetes. Feb 2007;56(2):363-372.
22. Jong MC, Dahlmans VE, van Gorp PJ, et al. In the absence of the low density lipoprotein receptor, human apolipoprotein C1 overexpression in transgenic mice inhibits the hepatic uptake of very low density lipoproteins via a receptor-associated protein-sensitive pathway. J Clin Invest. Nov 15 1996;98(10):2259-2267.
23. van Dam AD, Bekkering S, Crasborn M, et al. BCG lowers plasma cholesterol levels and delays atherosclerotic lesion progression in mice. Atherosclerosis. Aug 2016;251:6-14.
24. Sison K, Eremina V, Baelde H, et al. Glomerular structure and function require paracrine, not autocrine, VEGF-VEGFR-2 signaling. J Am Soc Nephrol. Oct 2010;21(10):1691-1701.
25. Mosser DM, Zhang X. Activation of murine macrophages. Curr Protoc Immunol. Nov 2008;Chapter 14:Unit 14 12.
26. Tervaert TW, Mooyaart AL, Amann K, et al. Pathologic classification of diabetic nephropathy. J Am Soc Nephrol. Apr 2010;21(4):556-563.
27. Pagtalunan ME, Miller PL, Jumping-Eagle S, et al. Podocyte loss and progressive glomerular injury in type II diabetes. J Clin Invest. Jan 15 1997;99(2):342-348.
28. Anders HJ, Ryu M. Renal microenvironments and macrophage phenotypes determine progression or resolution of renal inflammation and fibrosis. Kidney Int. Nov

2011;80(9):915-925.

29. Berbee JF, Coomans CP, Westerterp M, et al. Apolipoprotein CI enhances the biological response to LPS via the CD14/TLR4 pathway by LPS-binding elements in both its N- and C-terminal helix. J Lipid Res. Jul 2010;51(7):1943-1952.
30. Bouillet B, Gautier T, Aho LS, et al. Plasma apolipoprotein C1 concentration is associated with plasma triglyceride concentration, but not visceral fat, in patients with type 2 diabetes. Diabetes Metab. Sep 2016;42(4):263-266.
31. Klessens CQ, Woutman TD, Veraar KA, et al. An autopsy study suggests that diabetic nephropathy is underdiagnosed. Kidney Int. Jul 2016;90(1):149-156.
32. Westerterp M, de Haan W, Berbee JF, et al. Endogenous apoC-I increases hyperlipidemia in apoE-knockout mice by stimulating VLDL production and inhibiting LPL. J Lipid Res. Jun 2006;47(6):1203-1211.
33. Hattori M, Nikolic-Paterson DJ, Miyazaki K, et al. Mechanisms of glomerular macrophage infiltration in lipid-induced renal injury. Kidney Int Suppl. Jul 1999;71:S47-50.
34. Gustavsson C, Agardh CD, Zetterqvist AV, et al. Vascular cellular adhesion molecule-1 (VCAM-1) expression in mice retinal vessels is affected by both hyperglycemia and hyperlipidemia. PLoS One. 2010;5(9):e12699.
35. Chana RS, Martin J, Rahman EU, et al. Monocyte adhesion to mesangial matrix modulates cytokine and metalloproteinase production. Kidney Int. Mar 2003;63(3):889-898.
36. Madge LA, Pober JS. TNF signaling in vascular endothelial cells. Exp Mol Pathol. Jun 2001;70(3):317-325.
37. Ostendorf T, Kunter U, Grone HJ, et al. Specific antagonism of PDGF prevents renal scarring in experimental glomerulonephritis. J Am Soc Nephrol. May 2001;12(5):909-918.
38. Stefanidis I, Kreuer K, Dardiotis E, et al. Association between the interleukin-1beta Gene (IL1B) C-511T polymorphism and the risk of diabetic nephropathy in type 2 diabetes: a candidate-gene association study. DNA Cell Biol. Jul 2014;33(7):463-468.
39. Lai KN, Leung JC, Chan LY, et al. Podocyte injury induced by mesangial-derived cytokines in IgA nephropathy. Nephrol Dial Transplant. Jan 2009;24(1):62-72.
40. Schiffer M, Bitzer M, Roberts IS, et al. Apoptosis in podocytes induced by TGF-beta and Smad7. J Clin Invest. Sep 2001;108(6):807-816.
41. Paueksakon P, Revelo MP, Ma LJ, et al. Microangiopathic injury and augmented PAI-1 in human diabetic nephropathy. Kidney Int. Jun 2002;61(6):2142-2148.
42. Hamsten A, Silveira A, Boquist S, et al. The apolipoprotein CI content of triglyceride-rich lipoproteins independently predicts early atherosclerosis in healthy middle-aged men. J Am Coll Cardiol. Apr 5 2005;45(7):1013-1017.
43. Noto AT, Mathiesen EB, Brox J, et al. The ApoC-I content of VLDL particles is associated with plaque size in persons with carotid atherosclerosis. Lipids. Jul 2008;43(7):673-679.
44. Westerterp M, Berbee JF, Pires NM, et al. Apolipoprotein C-I is crucially involved in lipopolysaccharide-induced atherosclerosis development in apolipoprotein E-knockout mice. Circulation. Nov 6 2007;116(19):2173-2181.
45. Hirano T, Sakaue T, Misaki A, et al. Very low-density lipoprotein-apoprotein CI is increased in diabetic nephropathy: comparison with apoprotein CIII. Kidney Int. Jun 2003;63(6):2171-2177.
46. Kannel WB, McGee DL. Diabetes and cardiovascular risk factors: the Framingham study. Circulation. Jan 1979;59(1):8-13.

Supplementary Materials

Table S1: Absolute and relative organ weights in WT and *APOC1*-tg mice at 6 months of age.

	WT	*APOC1*-tg	WT	*APOC1*-tg
Organ	**Weight, grams (mean±SD)**	**Weight grams (mean±SD)**	**Relative weight, % (mean±SD)**	**Relative weight % (mean±SD)**
Kidney (left)	0.16±0.03	0.18±0.04	0.56±0.04	0.64±0.09**
Kidney (right)	0.17±0.03	0.18±0.03	0.57±0.04	0.66±0.09***
Heart	0.15±0.03	0.20±0.03	0.52±0.04	0.58±0.07*
Liver	1.36±0.25	1.27±0.25	4.62±0.19	4.55±0.58
Brain	0.33±0.02	0.34±0.04	1.16±0.21	1.24±0.20
Lungs	0.18±0.01	0.19±0.03	0.64±0.12	0.68±0.13
Spleen	0.09±0.01	0.10±0.02	0.32±0.07	0.38±0.10
Pancreas	0.28±0.07	0.26±0.05	0.96±0.18	0.95±0.17
Total Body Weight	29.4±5.0	27.9±4.3	NA	NA

*$p<0.05$, **$p<0.01$, and ***$p<0.001$ versus WT; Student's *t* test. NA, not applicable.

Table S2: Laboratory values of WT and *APOC1*-tg mice at 6 months of age.

	WT	*APOC1*-tg
Triglycerides (mmol/L)	0.58±0.06	2.83±0.97***
Total cholesterol (mmol/L)	2.33±0.28	3.88±0.91***
HDL-C (mmol/L)	2.14±0.33	2.33±0.64
Non-HDL-C (mmol/L)	0.19±0.13	1.56±0.49***
GOT (U/L)	$0.2\pm0.1x10^{-3}$	$0.1\pm0.06x10^{-3}$
CK (U/L)	$1.2\pm0.1x10^{-3}$	$1.4\pm0.8x10^{-3}$
Haemoglobin (mmol/L)	11.03±0.71	10.91±0.72
White blood cells ($x10^9$)	2.607±0.59	2.391±0.30
BUN (mg/dl)	31.25±6.76	27.19±5.18
Serum creatinine (µmol/L)	11.0±2.7	13.0±2.8
Blood glucose (mmol/L)	11.83±1.60	11.42±2.54

Data are presented as the mean ± sd. HDL-C, high-density lipoprotein cholesterol; BUN, blood urea nitrogen; GOT, glutamate oxaloacetate transaminase; CK, creatinine kinase. *$p<0.05$, **$p<0.01$, and ***$p<0.001$ versus WT, Student's *t* test.

Table S3: Summary of patient and control subjects used for human apoCI staining.

	Autopsy control (n=17)	DM, no DN (n=8)	DM, with DN (n=12)
Age (years)	65±12	76±12	72±9
DM duration (years)	NA	12±10	23±13
HbA1c (%)	NA	7.4±0.26	7.9±0.84
Serum creatinine (µmol/ml)	NA	310±282	310±141
Blood pressure (systolic/diastolic)	NA	137/73	134/79

Data are presented as the mean ± sd; blood pressure is presented as the mean value. DM, diabetes mellitus; DN, diabetic nephropathy; NA, not applicable.

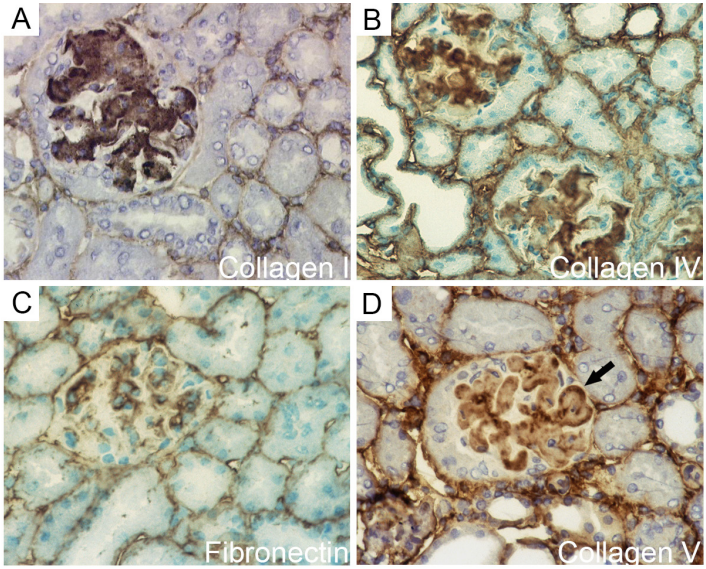

Figure S1: Sclerotic lesions contain deposits of collagen type I, collagen type IV, collagen type VI, and fibronectin. Glomerulosclerotic lesions in a 16-month-old *APOC1*-tg mice have an intense staining pattern for the extracellular matrix (ECM) proteins collagen type I (A), collagen type IV (B), and fibronectin (C). Collagen type VI is also present in the sclerotic lesions (D), but only in the peripheral areas (arrow).

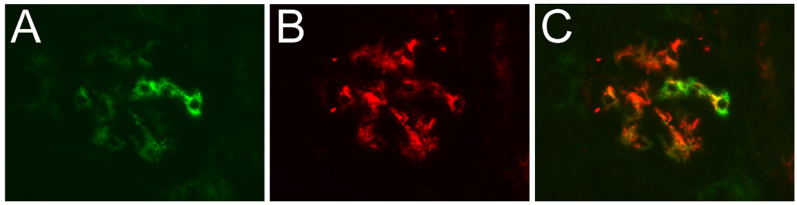

Figure S2: VCAM-1 expression in endothelial cells. A-C. Double-label immunostaining for VCAM-1 (A) and von Willebrand factor (B) in the kidneys of a 16-month-old *APOC1*-tg mouse, showing co-localisation exclusively in endothelial cells (C).

Supplemental Methods

PAS, Silver, and Sirius Red staining

Paraffin-embedded sections (4 µm thickness) were oxidised in periodic acid at 48°C for 30 minutes, then washed with demi-water. The sections were then incubated in 5% Schiff's reagent for 20 minutes, incubated in tap water for 5 minutes, then rinsed briefly in demi-water. Finally, the sections were incubated in haematoxylin for 5 minutes, followed by incubation in tap water for 5 minutes.

For silver staining, paraffin-embedded sections (1-µm thickness) were cut and incubated in 1% periodic acid for 10 minutes at 60°C, and then stained in a silver solution at 60°C until the glomerular basement membranes became black. The sections were then incubated in 0.2% gold chloride until the sections became light grey. Finally, the sections were incubated for 2 minutes in 5% sodium thiosulfate, 10 minutes in tap water, and 30 seconds in eosin.

Paraffin-embedded sections were stained with Sirius Red by incubating sections with 0.2% phosphomolybdic acid for 5 minutes, 0.1% Sirius Red for 90 minutes, and saturated picric acid for 1 minute.

Primer sequences

Hprt1: 5'-GGCTATAAGTTCTTTGCTGACCTG-3' and 5'-AACTTTTATGTCCCCCGTTGA-3'; human *APOC1*: 5'-AGCCGCATCAAACAGAGTGA-3' and 5'-TCCTGGGATGTCACCCTTCA-3'; mouse *ApoC1*: 5'- GTCCGGAACATTGGAGAGCA-3' and 5'-CCTGAAAGGTCCTAACCGGG-3'; mouse *Tnf-alpha*: 5'-GGTGCCTATGTCTCAGCCTC-3' and 5'-GCTCCTCCACTTGGTGGTTT-3'; mouse *Tgf-beta*: 5'-AGCTGCGCTTGCAGAGATTA-3' and 5'-AGCCCTGTATTCCGTCTCCT-3'; mouse *Pdgf-beta*: 5'-TGTGAGACAGTAGTGACCCCT-3' and 5'-AAACTTTCGGTGCTTGCCTTT-3'; mouse *Il1-beta*: 5'-GCTCTCCACCTCAATGGACA-3' and 5'-GTGGGTGTGCCGTCTTTCAT-3'.